Structural Engineering and Mechanics, Vol. 14, No. 1 (2002) 39-56
DOI: http://dx.doi.org/10.12989/sem.2002.14.1.039

Optimal distribution of the cable tensions and structural vibration control of the cable-cabin flexible structure

Y.Y. Qiu†, B.Y. Duan‡ and Q. Wei‡†

School of Mechanical and Electronic Engineering, Xidian University, Xi'an, 710071, China

R.D. Nan‡ and B. Peng‡

Beijing Radio Astronomy Observatory, Chinese Academy, Beijing, 100012, China

(Received February 2, 2001, Accepted April 23, 2002)

Abstract: In order to trace a target in deep sky, a feed cabin 20 tons in weight used for a large radio telescope is drawn with six cables. To realize a smooth tracing all the time, optimal distribution of the cable tensions is explored. A set of cable-clog systems is utilized to control the wind-induced vibration of the cable-cabin structure. This is an attempt to apply the passive structural control strategy in the area of radio astronomy. Simulations of wind-induced vibration of the structure in both time and frequency domains offer a valuable reference for construction of the next generation large radio telescope.

Key words: large radio telescope; cable-cabin structure; optimization; wind-induced vibration; passive structural control; nonlinear analysis.

1. Introduction

The world's largest radio telescope (LT) is hopefully to be built in KARST area of Guizhou Province of China in near future (Li 1998). Since the spherical reflector 500 meters in caliber was too large to rotate, unlike reflectors of traditional radio telescopes, the reflector was set on a natural limestone depression surrounded by hills over two hundred meters high. On the contrary, the cable towers were erected on the hills and a line feed 20 tons in weight was drawn with six cables to trace an object moving across the sky (Duan 1999).

According to scientific object of LT, the receiving frequencies of electromagnetic waves of LT are demanded to cover a wide bandwidth from 0.3 GHz to 8.8 GHz. However, there is a strict constraint of the bandwidth if a line feed is utilized. For the sake of this, an active reflector design concept was proposed (Duan 1999). The line feed was replaced by nine multi-beam point feeds with different bandwidths. These point feeds were amounted in a cabin drawn with six cables.

† Associate Professor
‡ Professor
‡† Ph.D. Student

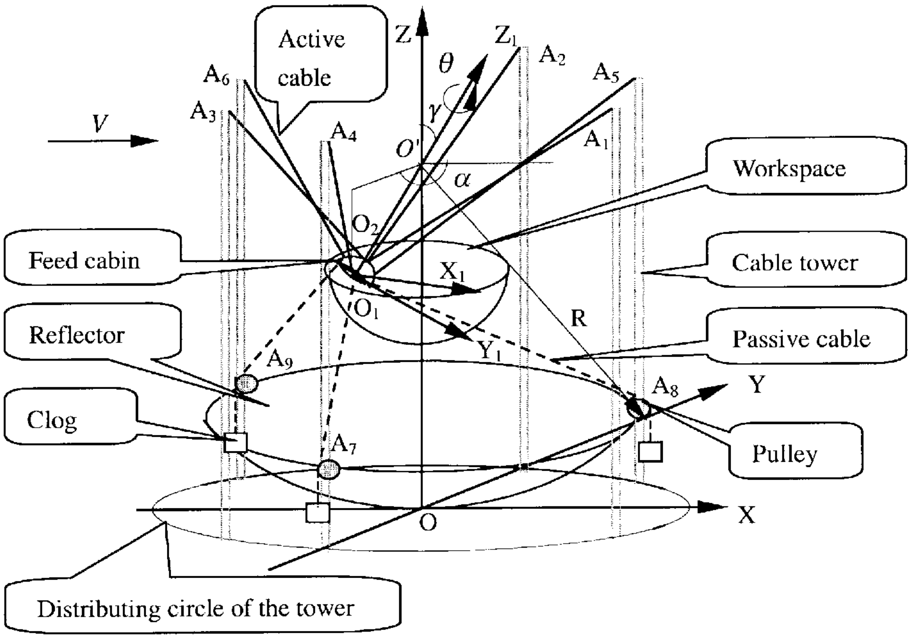

Fig. 1 Improved model of LT with a feed cabin

Correspondingly thousands of hexagonal panels were put together forming the spherical reflector and each hexagonal panel could be adjusted by the hydraulic devices independently. When a working point feed tracing the selected target, those illuminated hexagonal panels form a local parabolic reflector with 300 meters in caliber. With the movement of the working point feed, new local parabolas were generated continually. Fig. 1 presents the improved model of LT with a feed cabin.

The cable tensions are asked to make sure that the radio source (target) is always aimed and traced nicely and smoothly. It is necessary to find an optimal distribution of the cable tensions. In this way, the six servomotors controlled by a central computer will work in a good condition and the position and orientation of the cabin can be kept stable.

Since the cabin is suspended with six computer-controlled long cables, the stiffness of the cabin-cable structure is pretty low. In addition, the cabin may move away from its desired position and orientation under disturbances, for instance, random wind. The most common used control devices for tall buildings and high-rise structures are active and passive tuned mass dampers (ATMD and TMD) (Li and Cao 1999). Besides, inclined cables with lower ends fixed on bases are also used for high-rise structures such as guyed towers and guyed masts. However the cabin has not enough space to hold a TMD, and unlike stationary high buildings and high-rise structures, the feed cabin has to move slowly to trace a target which does not allow the inclined cables with fixed ends. So the traditional structural control methods mentioned above are not appropriate for the situation here.

On the one hand, the wind-induced vibration of the structure must be reduced. On the other hand, the passive cables should not hinder the specified movement of the cabin. As a result, three sets of passive cable-clog systems are added into the structure symmetrically as shown in Fig. 1. Each cable-clog system consists of a passive cable, a clog and a pulley. Taking account of their stiffness and damps, these cable-clog systems could be considered as three parallel TMD in general.

For a strong nonlinear structure, it is necessary to give an initial static reference posture of the structure to construct the geometry stiffness matrix before vibration analysis. In fact, this job has been made at the same time when we determine the optimal cable tensions by executing nonlinear static analysis of the cable-cabin structure.

2. Nonlinear static analysis of the structure

2.1 Workspace of the cabin

In Fig. 1, radius of curvature of the reflector is R with the center O'. According to the observing requirement, the cabin has to be moved on the surface of a spherical part with the radius of $0.533\,R$, centered at the center O'. During the observation, the local coordinate axis Z_1 of the cabin should always pass through the center O' and axis Y_1 should always intersect with axis Z. In this case, axis X_1 always keeps horizontal. α, γ, and ϑ are the orientation angles of the cabin. α is the angle between vertical planes $O_1Y_1Z_1$ and OXZ. γ is the angle between axes Z and Z_1. ϑ is the angle around axis Z_1. The maximum of γ is $\Phi/2$.

2.2 Equivalent equations on the cabin

In Fig. 1, towers $A_1 \sim A_6$ are distributed evenly on a circle with the diameter of D_1. The cables A_1B_1, A_2B_2, and A_3B_3 are connected from the top of the cabin to the towers A_1, A_2, and A_3 respectively. The other three cables A_4B_4, A_5B_5, and A_6B_6 are connected from the towers A_4, A_5, and A_6 to the points B_4, B_5 and B_6 of the cabin. In Fig. 2, B_1, B_2, and B_3 are overlapped at the top point O_2 of the cabin, and B_4, B_5, and B_6 are three even distributed points of the cabin.

Angle θ (Fig. 2) between O_1B_4 and O_1X_1 is the orientation angle of the cabin indicating the rotation of the cabin around its axis Z_1. Upon the global coordinates of the origin O_1 are known the orientation angles α and γ can be known too. However the orientation angle θ has to be found. It can be noted from Fig. 2 that the coordinates of B_4, B_5, and B_6 have relationships with θ, and the global coordinates of B_i can be obtained as follows,

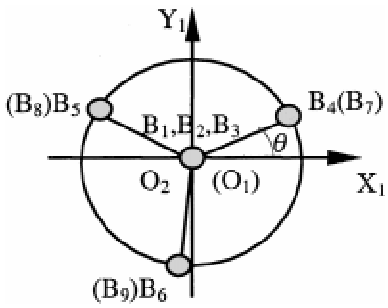

Fig. 2 Connection between the cables and the cabin

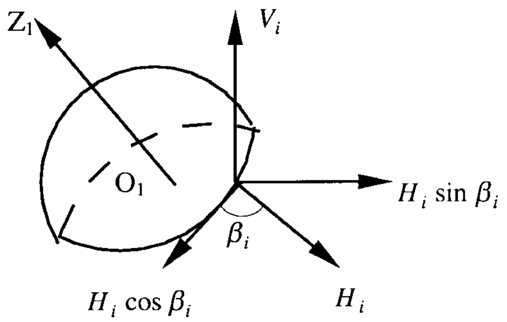

Fig. 3 Components of a cable tension with respect to the cabin

$$\boldsymbol{r}_i = [x_i \;\; y_i \;\; z_i]^T = \boldsymbol{r}_{O1} + \boldsymbol{Q}\boldsymbol{r}_{i1} \qquad (i = 1, 2, \ldots, 6) \tag{1}$$

where $\boldsymbol{r}_{O1}$ is the absolute vector of the origin O_1 in global coordinate system $OXYZ$, and $\boldsymbol{r}_{i1}$ is the relative vector of end B_i in local coordinate system $O_1X_1Y_1Z_1$. $\boldsymbol{Q}$ is the orientation matrix of the cabin related to α and γ. From definition on α and γ in section 2.1, $\boldsymbol{Q}$ can be found from,

$$\boldsymbol{Q} = \begin{bmatrix} s\alpha & c\alpha & 0 \\ -c\alpha & s\alpha & 0 \\ 0 & 0 & 1 \end{bmatrix} \begin{bmatrix} 1 & 0 & 0 \\ 0 & c\gamma & s\gamma \\ 0 & -s\gamma & c\gamma \end{bmatrix} = \begin{bmatrix} s\alpha & c\alpha c\gamma & c\alpha s\gamma \\ -c\alpha & s\alpha c\gamma & s\alpha s\gamma \\ 0 & -s\gamma & c\gamma \end{bmatrix} \tag{2}$$

where the expressions $c\alpha$ and $s\alpha$ stand for $\cos\alpha$ and $\sin\alpha$ respectively.

Each cable is located in a vertical. Supposing β_i is an angle between cable A_iB_i and the vertical plane OXZ, then β_i can be described by the coordinates of A_i and B_i. A cable tension F_i with respect to the cabin can be written in terms of $F_i = [H_i\cos\beta_i \;\; H\sin\beta_i V_i]^T$, in which H_i and V_i are the horizontal and vertical components of F_i separately as shown in Fig. 3.

Up to now, the equivalent equations on the feed cabin can be written as follows,

$$\left.\begin{aligned} &\sum_{i=1}^{9} H_i\cos\beta_i = 0 \\ &\sum_{i=1}^{9} H_i\sin\beta_i = 0 \\ &\sum_{i=1}^{9} V_i - W = 0 \\ &\sum_{i=1}^{9} (y_iV_i - z_iH_i\sin\beta_i) - W\cdot y_d = 0 \\ &\sum_{i=1}^{9} (z_iH_i\cos\beta_i - x_iV_i) + W\cdot x_d = 0 \\ &\sum_{i=1}^{9} (x_iH_i\sin\beta_i - y_iH_i\cos\beta_i) = 0 \end{aligned}\right\} \tag{3}$$

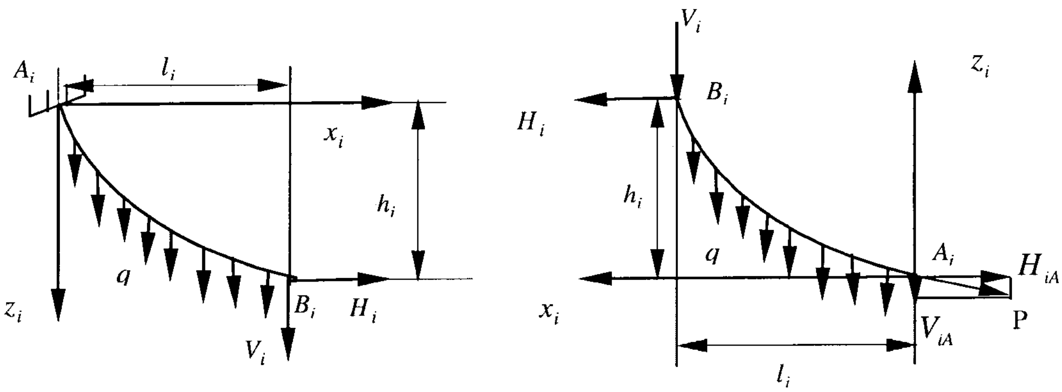

(a) Active cable $(i = 1,2, \ldots ,6)$ (b) Passive cable $(i = 7,8,9)$

Fig. 4 A cable in its local coordinate system

In which, W is the weight of the cabin. x_d and y_d are the coordinates of cabin's center of gravity in global coordinate system *OXYZ*.

2.3 Nonlinear equivalent equation on a cable

Each cable can be described in its local coordinate system $A_i x_i z_i$.

From Fig. 4(a), the equivalent equation of moment of each active cable with respect to its upper suspension point A_i is

$$H_i h_i - V_i l_i - \int_0^{l_i} q x_i \sqrt{1 + \dot{z}_i^2}\, dx_i = 0 \qquad (i = 1, 2, \ldots, 6) \tag{4}$$

Meanwhile, the equivalent equation of moment of each passive cable with respect to its lower end A_i (Fig. 4(b)) becomes,

$$H_i h_i + V_i l_i + \int_0^{l_i} q x_i \sqrt{1 + \dot{z}_i^2}\, dx_i = 0 \qquad (i = 7, 8, 9) \tag{5}$$

where q is the density of cable material. l_i and h_i are the vertical and horizontal projected lengths of the cable related to θ. $\dot{z}_i$ is a differentiation of z_i with respect to x_i, which can be obtained from the following equation (Wang 1999)

$$z_i = -\frac{H_i}{q}\cosh\left(\frac{x_i q}{H_i} + c_{2i}\right) + c_{1i} \qquad (i = 1, 2, \ldots, 9) \tag{6}$$

In which, integral constants c_{1i} and c_{2i} can be obtained from boundary conditions $A_i(0, 0)$ and $B_i(l_i, h_i)$.

In addition, the equivalent equations for three passive cables in the directions of the local axes x_i and z_i can be known respectively as follows,

$$\left.\begin{aligned} &H_i - H_{iA} = 0 \\ &V_i + V_{iA} + \int_0^{l_i} q\sqrt{1+\dot{z}_i^2}\,dx_i = 0 \end{aligned}\right\} \quad (i = 7, 8, 9) \tag{7}$$

Assuming that each clog has the same weight P, the tension at lower end A_i of each passive cable will satisfy the following equations,

$$V_{iA}^2 + H_{iA}^2 = P^2 \qquad (i = 7, 8, 9) \tag{8}$$

Combining Eqs. (5), (7) and (8), gives the following formulae,

$$h_i H_i + \int_0^{l_i} q x_i \sqrt{1+\dot{z}_i^2}\,dx_i - l_i\sqrt{P^2 - H_i^2} - l_i \int_0^{l_i} q\sqrt{1+\dot{z}_i^2}\,dx_i = 0 \qquad (i = 7, 8, 9) \tag{9}$$

2.4 Nonlinear equivalent equations on the cable-cabin structure

At any point within the workspace of the cabin, all six parameters X_{o1}, Y_{o1}, Z_{o1}, α, γ, and θ of the cabin are known except for θ. If θ is assumed suitably, the coordinates of each end B_i can be obtained correspondingly. Consequently, h_i and l_i can be found too. As a result, H_7, H_8, and H_9 can be obtained by least square method.

From Eqs. (4) and (5), the vertical component V_i of each cable tension at the cabin end can be expressed with H_i. Substituting this expression and H_7, H_8, and H_9 into Eq. (3) yields the following equation

$$\boldsymbol{A}(\theta)\boldsymbol{H}=\boldsymbol{B}(\theta) \tag{10}$$

where $\boldsymbol{A} \in R^{6\times 6}$ is a Jacobin matrix. $\boldsymbol{H} = [H_1\ H_2\ H_3\ H_4\ H_5\ H_6]^T$ is the vector describing the horizontal components of the active cable tensions. $\boldsymbol{B} \in R^{6\times 1}$ is the load vector acting on the structure.

2.5 Optimal distribution of the cable tensions

The six active cables are controlled with six computer-controlled servomotors. Since a cable can be subjected to tension only, the posture adjusting of the cabin will be constrained to a certain extent. In order to have a uniform tension distribution among the active cables, the following mathematical model is proposed,

$$\begin{aligned} \min f(\theta) &= \max F_i - \min F_i \ (i = 1, 2, ..., 6) \\ \text{s.t. } \boldsymbol{AH}(\theta) &= \boldsymbol{B}(\theta) \\ H_i &> 0 \end{aligned} \tag{11}$$

where constraint $H_i > 0$ ensures the cables state under tension. It should be noted that $F_i = \sqrt{V_i^2 + H_i^2}$.

2.6 Numerical simulation results

Suppose that the diameter of distribution circle of the towers $Dt = 500$ m, the heights of the active and passive cable's towers $Ta = 250$ m and $Tp = 73$ m respectively, the caliber of the spherical reflector $D = 400$ m, the taper angle $\Phi = 80^{\circ}$, the orientation angles $\alpha = 0^{\circ}$ and $\gamma = 15^{\circ}$ (Fig. 1 and Fig. 5). The weights of the cabin and each clog $Q = 20$ t and $P = 1$ t respectively. The radius of curvature of the reflector will be,

$$R = \frac{D/2}{\sin(\Phi/2)} \tag{12}$$

The coordinates of a point p within workspace of the cabin will be,

$$x_P = 0.533\, R\sin\gamma\cos\alpha, \quad y_P = 0.533\, R\sin\gamma\sin\alpha \quad \text{and} \quad z_P = R(1 - 0.533\cos\gamma) \tag{13}$$

It should be noted that the weight of each clog should be large enough to balance the weight of the corresponding passive cable. On the other hand, considering powers of the servomotors, the

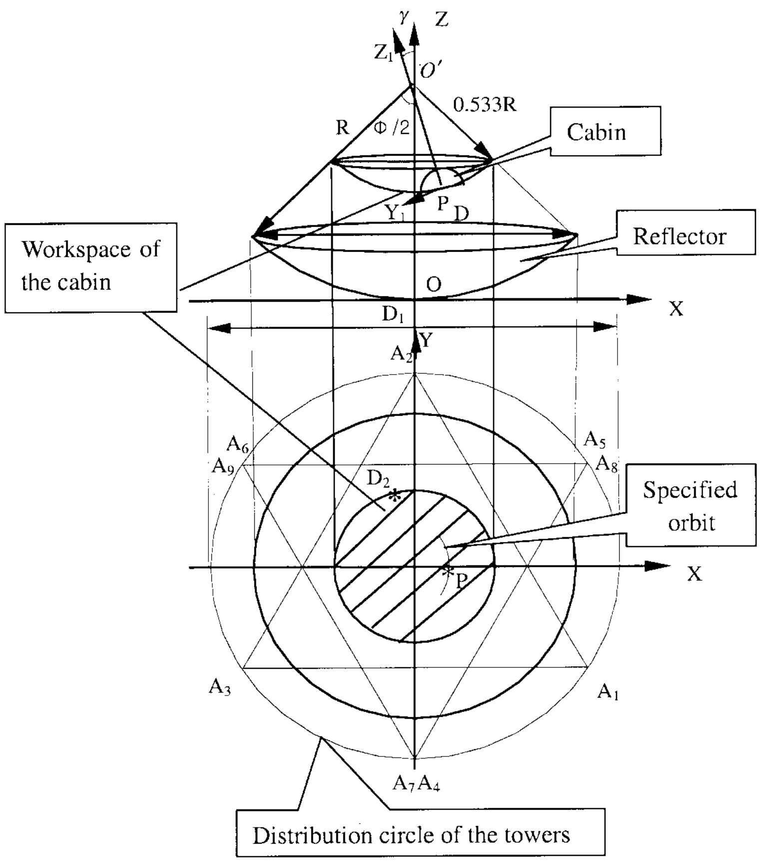

Fig. 5 Sketch map for numerical simulation

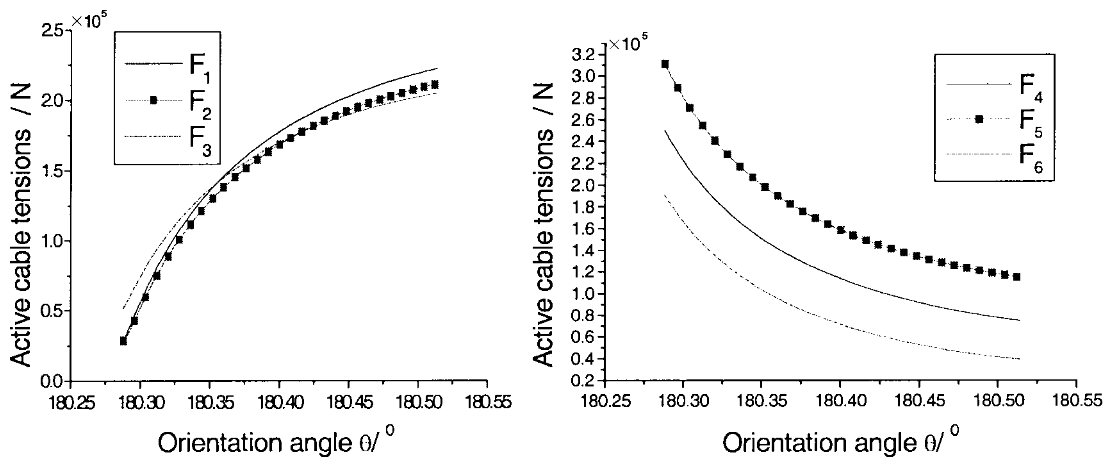

Fig. 6 Variations of the active cable tensions with the orientation angle θ

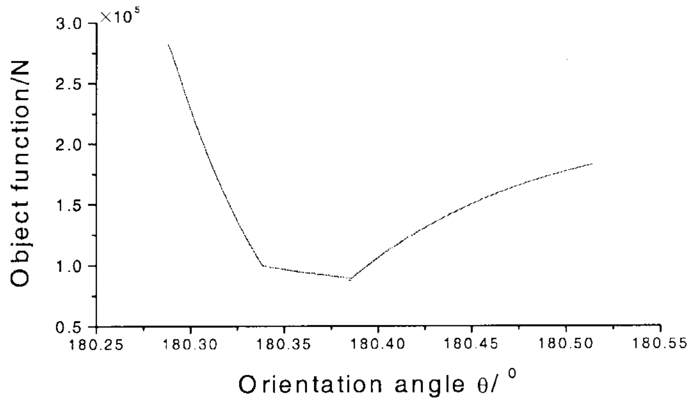

Fig. 7 Object function

weight of the clog should not be too large. Under these conditions, the optimal results of the active cable tensions are drawn in Fig. 6, and the corresponding object function is described in Fig. 7.

In Fig. 6 and Fig. 7, the horizontal axes describe parameter θ whilst the vertical axes show the active cable tension F_i and the object function given by formula (11) respectively. From Fig. 6, it can be noted that the cable tensions are varying with θ, particularly within $[180.28^{\circ}\ \ 180.52^{\circ}]$. For instance, $F_{1\max}$ is seven times as large as $F_{1\min}$. In order to have a smooth movement of the cabin, it is necessary to optimize the distribution of cable tensions. In Fig. 7, object function reaches its minimum when $\theta = 180.38^{\circ}$. Obviously, we should select it as the final selection of the cable tensions.

Further supposing that the orientation angles $\gamma \equiv 15^{\circ}$ and α varies within $[-20^{\circ}\ \ 20^{\circ}]$ whilst the other parameters have the same values as above, the horizontal component H_i of the cable tensions are shown in Fig. 8. In which, the horizontal axis describes α, and the vertical axis describes $H_1 \sim H_9$. The smooth optimal tensions are suitable for servomotor control.

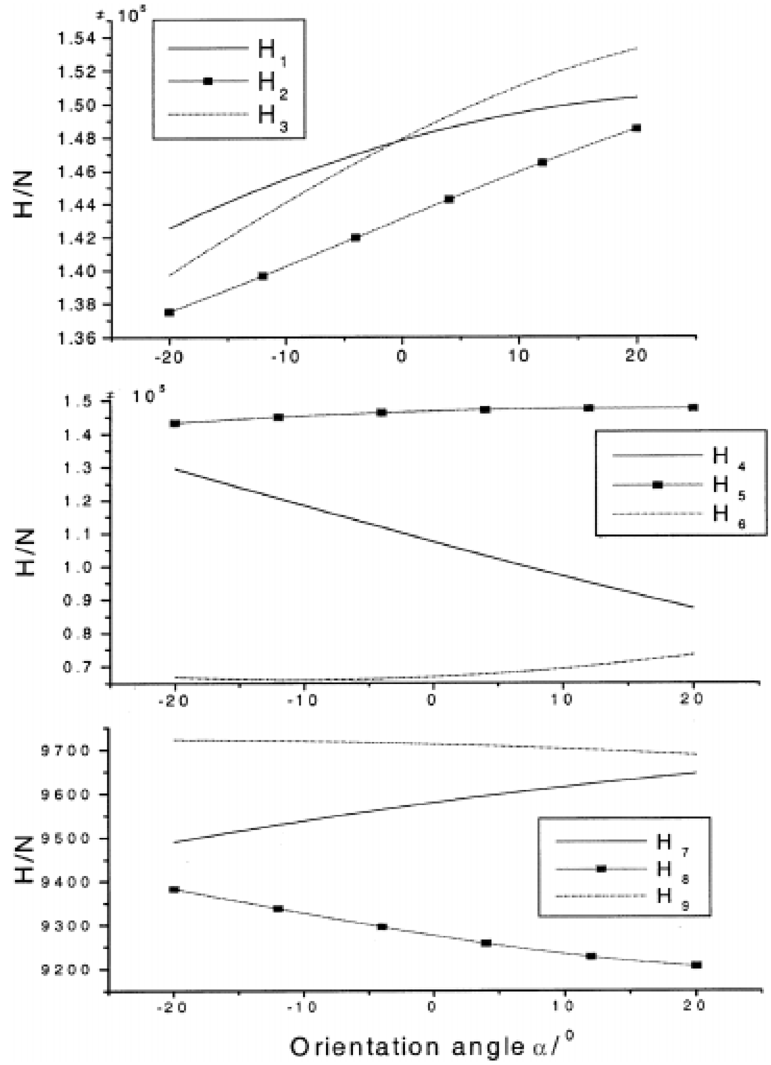

Fig. 8 Horizontal tensions of the cables for the specified orbit

3. Wind-induced vibration of the cable-cabin structure

3.1 Simulation of the wind velocity

Aerodynamic forces acting on structures arise from the superposition of static loads due to mean wind and fluctuating loads due to gusts. Thus a wind velocity may be decomposed into

$$V(x, y, z, t) = \overline{V}(z) + v(x, y, z, t) \tag{14}$$

where $v(x, y, z, t)$ is a fluctuating velocity and $\overline{V}(z)$ is a mean velocity at height z satisfying the exponential law:

$$\bar{V}(z) = \bar{V}_{10}(z/10)^{\alpha} \tag{15}$$

in which $\bar{V}_{10}$ indicates the mean velocity at 10 meters high; α is a coefficient related to the ground roughness.

Davenport spectrum of a horizontal fluctuating velocity is:

$$S_V(f) = 4K\bar{V}_{10}^2 \frac{X^2}{f \cdot (1+X^2)^{4/3}}, \quad X = \frac{L_v^* f}{\bar{V}_{10}} \tag{16}$$

where K is a roughness coefficient and L_V^* is the integral scale of turbulence. From formula (16), mean square value of a fluctuating velocity can be deduced

$$\psi_V^2 = R_V(0) = 2\int_0^{\infty} S_V(f)df = 0.18\bar{V}_{10}^2 \tag{17}$$

Usually a fluctuating velocity is considered as a Gaussian process with a zero mean, so its standard deviation may be obtained as follows:

$$\sigma_V = \sqrt{\psi_V^2 - \mu^2} \approx 0.424\bar{V}_{10} \tag{18}$$

The cable-cabin structure is likely to be a high-rise structure, and Davenport spectrum does not vary with height, so Maier spectrum related to height z is introduced as,

$$S_V(z, f) = \frac{2X^2}{(1+3X^2)^{4/3}} \cdot \frac{\sigma_V^2(z)}{f}, \quad X = L_V^* \frac{f}{\bar{V}(z)} \tag{19}$$

The cross-power spectrum of a fluctuating velocity could be written as follows (Wang 1994):

$$\left.\begin{aligned}
S_{xy}(f) &= \sqrt{S_{xx}(f)S_{yy}(f)} \cdot ch(f) \cdot e^{i\psi(f)} \\
ch(f) &= \exp\left(-\frac{C_z \cdot f \cdot \Delta z}{\bar{V}(z)}\right) \\
\bar{V}(z) &= \bar{V}_{10}\left(\frac{z}{10}\right)^{0.16} \\
\psi(f) &= \begin{cases} \frac{\pi}{4} \cdot \frac{f\Delta z}{\bar{V}(z)} & \frac{f\Delta z}{\bar{V}(z)} \le 0.1 \\ -10\pi\frac{f\Delta z}{\bar{V}(z)} + 1.25 & 0.1 < \frac{f\Delta z}{\bar{V}(z)} \le 0.125 \\ \text{random variable} & \frac{f\Delta z}{\bar{V}(z)} > 0.125 \end{cases}
\end{aligned}\right\} \tag{20}$$

in which C_Z is an exponential decay coefficient and Δz is the height difference between two points.

Further the matrix of power spectral density can be given as (Wang 1994)

$$\underline{S}(\omega) = \begin{bmatrix} S_{11}(\omega) & \dots & S_{1n}(\omega) \\ \dots & \dots & \dots \\ S_{n1}(\omega) & \dots & S_{nn}(\omega) \end{bmatrix} = H(\omega)[H^*(\omega)]^T \tag{21}$$

in which $\omega = 2\pi f$ and $H(\omega)$ is a triangle matrix gotten from Cholesky decomposition of matrix $\underline{S}(\omega)$.

Up to now, the along-wind velocity is simulated as follows (Wang 1994):

$$V_j(x, y, z, t) = \bar{V}_j(z) + \sum_{m=1}^{j} \sum_{l=1}^{N} |H_{jm}(\omega)| \sqrt{2\Delta\omega} \cos[\omega_l \cdot t + \psi_{jm}(\omega_l) + \theta_{ml}] \quad j = 1, 2, \dots, n \tag{22}$$

in which $\bar{V}_j(z)$ is the mean wind velocity at jth height; n and N denote the numbers of divided segments uniformly along the structural height and in frequency band of the wind velocity spectrum respectively; $\Delta\omega$ is a frequency increment; $\psi_{jm}(\omega_l)$ refers to a phase angle related to two points at different heights; θ_{ml} is a random variable ranging from 0 to 2π. In this paper, the wind-induced vibration caused by the along-wind velocity is considered especially.

The wind pressure can be simulated as follows:

$$\omega(x, y, z, t) = \frac{1}{2}\rho V^2(x, y, z, t) = \frac{1}{2}\rho[\bar{V}(z) + v(x, y, t)]^2 \tag{23}$$

where ρ is the air density.

3.2 Simulation of the wind forces acting on a cable

Each cable is divided into a group of cable bars with a length about 8 meters long. Assuming the vertical projection length of ith cable element is equal to h_i; The diameter of the cable is d and the incidence angle of wind velocity with respect to ith cable element is φ_i. The horizontal and vertical components of the wind force acting on the ith cable element can be expressed as (Zhang 1985):

$$\left.\begin{aligned} F_{Hi} &= \mu_{Hi\ cable}\,\omega d h_i \\ F_{Vi} &= \mu_{Vi\ cable}\,\omega d h_i \end{aligned}\right\} \tag{24}$$

where the coefficients $\mu_{Hi\ cable}$ and $\mu_{Vi\ cable}$ are related to the angle φ_i.

3.3 Simulation of the wind forces acting on the cabin

3.3.1 Decomposition of the wind velocity

Suppose the tilt cabin lies at a point within the workspace and the horizontal wind blows in the direction of global axis X as shown in Fig. 1. To convenient the simulation, the wind velocity V is decomposed along local axes X_1, Y_1, and Z_1 of the cabin, i.e.,

$$V_{X1} = V\sin\alpha, \quad V_{Y1} = V\cos\alpha\cos\gamma, \quad V_{Z1} = V\cos\alpha\sin\gamma \tag{25}$$

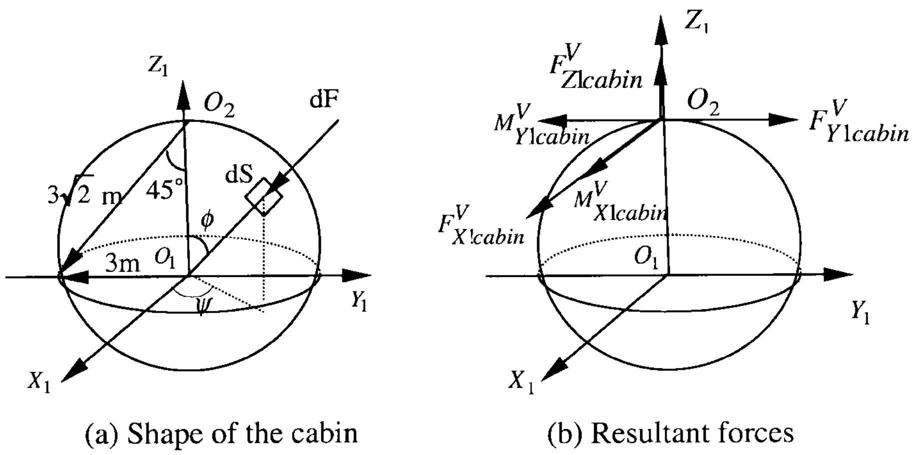

Fig. 9 Resultants wind forces acting on the cabin

A hemisphere with the radius of 3 meters, centered at O_1, and a spherical shell with $3\sqrt{2}$ meters in radius, centered at O_2, form the cabin as shown in Fig. 9. The shape coefficients of the hemisphere and the spherical shell are given as (Zhang 1985)

$$\left.\begin{aligned} \mu_{hemi} &= 0.5\sin^2\phi\sin\psi - \cos^2\phi \quad \text{for hemisphere} \\ \mu_{shell} &= -\cos^2\phi \quad \text{for spherical shellt} \end{aligned}\right\} \tag{26}$$

3.3.2 Wind forces caused by V_{Y1}

Since the rigidity of the cabin is much larger than that of the cables, it is reasonable to consider the cabin as a rigid to find the resultant wind forces acting on it before making finite element analysis for the cable-cabin structure.

Considering Eqs. (23), (25), and (26), the wind forces acting on the hemisphere caused by V_{Y1} can be replaced by three equivalent forces acting at the center O_1 by integrating on the surface of the hemisphere. Being dF as shown in Fig. 9(a) is a normal force, the equivalent forces are calculated by:

$$F_{X1hemi}^{Y1} = \int_s \mu_{hemi}\omega^{Y1}\sin\phi\cos\psi ds = 0 \tag{27}$$

$$\begin{aligned} F_{Y1hemi}^{Y1} &= \int_s \mu_{hemi}\omega^{Y1}\sin\phi\sin\psi ds \\ &= \int_0^{\pi/2}\int_0^{2\pi}(0.5\sin^2\phi\sin\psi - \cos^2\phi)\,\omega^{Y1}\sin\phi\sin\psi(R^2\sin\phi)d\psi\cdot d\phi \\ &= \frac{3\pi}{16}\cdot\frac{\pi R^2\omega^{Y1}}{2} \\ &= \frac{3\pi^2R^2\rho}{64}[\bar{V}(z) + v(x,y,z,t)]^2\cos^2\alpha\cos^2\gamma \end{aligned} \tag{28}$$

$$F_{Z1hemi}^{Y1} = \int_s \mu_{hemi} \omega^{Y1} \cos\phi ds$$

$$= -\frac{\pi R^2 \rho}{4} [\bar{V}(z) + v(x, y, z, t)]^2 \cos^2\alpha \cos^2\gamma \tag{29}$$

in Eqs. (27)-(29), the subscripts $X1_{hemi}$, $Y1_{hemi}$, and $Z1_{hemi}$ of F refer to the directions of the equivalent forces acting on the hemisphere, and the superscript $Y1$ means that the force is caused by V_{Y1}. ω^{Y1} denotes the wind pressure caused by V_{Y1}.

Since symmetry, F_{X1hemi}^{Y1} becomes zero. In Eq. (28), the coefficient $3\pi/16 \approx 0.589 < 1$, it indicates that the shape of the hemisphere is of benefit for decreasing the wind forces acting on the cabin. $F_{Z1hemi}^{Y1} < 0$ means that F_{Z1hemi}^{Y1} does not press the cabin down and on the contrary draws it up.

Similarly the wind forces acting on the surface of the shell caused by V_{Y1} can also be replaced by three equivalent forces acting at the center O_2 by integrating on the surface of the shell:

$$F_{X1shell}^{Y1} = \int_s \mu_{shell} \omega^{Y1} \sin\phi \cos\psi ds = 0 \tag{30}$$

$$F_{Y1shell}^{Y1} = \int_s \mu_{shell} \omega^{Y1} \sin\phi \sin\psi ds = 0 \tag{31}$$

$$F_{Z1shell}^{Y1} = \int_s \mu_{shell} \omega^{Y1} \cos\phi ds$$

$$= -\frac{3\pi R^2 \rho}{8} [\bar{V}(z) + v(x, y, z, t)]^2 \cos^2\alpha \cos^2\gamma \tag{32}$$

By executing the similar way, we can also have the equivalent forces acting at O_1 and O_2 caused by V_{X1} respectively.

3.3.3 Wind force caused by V_{Z1}

V_{Z1} has the same direction as local axis Z_1 does. Taking the shape coefficient $\mu_{cabin} = 1.3$ yields the following equivalent force caused by V_{Z1} acting on the whole cabin,

$$F_{X1cabin}^{Z1} = 0 \tag{33}$$

$$F_{Y1cabin}^{Z1} = 0 \tag{34}$$

$$F_{Z1cabin}^{Z1} = \frac{13\pi R^2 \rho}{20} [\bar{V}(z) + v(x, y, z, t)]^2 \cos^2\alpha \sin^2\gamma \tag{35}$$

where the subscript '*cabin*' means that the calculation is made for the whole cabin.

3.3.4 Resultants of the wind forces

From Eqs. (27)-(35), all the equivalent forces obtained above can be further combined into three forces and two moments acting at O_2, i.e., resultant forces caused by V as shown in Fig. 9(b),

$$F^V_{X1cabin} = \frac{3\pi^2 R^2 \rho}{64}[\bar{V}(z) + v(x, y, z, t)]^2 \sin^2\alpha \cdot \mathrm{sgn}(\sin\alpha) \tag{36}$$

$$F^V_{Y1cabin} = \frac{3\pi^2 R^2 \rho}{64}[\bar{V}(z) + v(x, y, z, t)]^2 \cos^2\alpha \cdot \cos^2\gamma \cdot \mathrm{sgn}(\cos\alpha) \tag{37}$$

$$F^V_{Z1cabin} = \frac{\pi R^2 \rho}{4}[\bar{V}(z) + v(x, y, z, t)]^2 \left(\frac{13}{5}\cos^2\alpha \cdot \sin^2\gamma \cdot \mathrm{sgn}(\cos\alpha) - \frac{1}{2}\cos^2\alpha \cdot \cos^2\gamma - \frac{1}{2}\sin^2\alpha\right) \tag{38}$$

$$M^V_{X1cabin} = F^{Y1}_{Y1hemi} \cdot R \tag{39}$$

$$M^V_{Y1cabin} = -F^{X1}_{X1hemi} \cdot R \tag{40}$$

Since the projection of the origin O_1 on horizontal plane OXY may be at any quadrant, sign functions sgn(sinα) and sgn(cosα) are introduced into the above Eqs. (36)-(38).

Let $\boldsymbol{F}^V_{XYZ1cabin} = [F^V_{X1cabin}, F^V_{Y1cabin}, F^V_{Z1cabin}, M^V_{X1cabin}, M^V_{Y1cabin}, 0]^T$ represent a vector of the wind forces acting on the cabin in local coordinate system. The vector can be transformed from local coordinate system to global coordinate system as,

$$\boldsymbol{F}^V_{XYZcabin} = \boldsymbol{Q}\boldsymbol{F}^V_{XYZ1cabin} \tag{41}$$

where $\boldsymbol{Q}$ is the orientation matrix of the cabin given in Eq. (2).

4. Simulation of wind-induced vibration of the cable-cabin structure

4.1 FEA model of the cable-cabin structure

Each cable is divided into a group of cable bars about 8 meters long. The frame structure of the cabin consists of 96 aluminum bar elements and 27 steel beam elements respectively.

If all six servomotors are braked, the cable-cabin mechanism will become a structure. When the origin O_1 of local coordinate system of the cabin is at point D_2(–30.263, 95.268, 191.929) (m) (in Fig. 5) and the orientation angles $\alpha = -107^o37'$, and $\gamma = 39^o59'$, the cabin reaches a boundary point of its workspace. At such a position and orientation, the structure is unsymmetrical badly, so the structural stiffness will be quite weakness. Choosing D_2 as a typical point, the wind-induced vibrations of the six-cable structure and the improved nine-cable structure are simulated and compared.

Table 1 Natural frequencies of the structure (HZ)

Order of the frequencies	Six-cable structure	Nine-cable structure
1	0.03057	0.04614
2	0.05235	0.07677
3	0.05868	0.08960
4	0.08032	0.1027
5	0.08473	0.1104

4.2 Dynamic equation of the cable-cabin structure

Dynamic equation of the cable-cabin structure is

$$\boldsymbol{M}\ddot{\boldsymbol{\delta}} + \boldsymbol{C}\dot{\boldsymbol{\delta}} + \boldsymbol{K}\boldsymbol{\delta} = \boldsymbol{F} \tag{42}$$

where $\boldsymbol{\delta}$ and $\boldsymbol{F}$ denot the displacement of the structral nodes and the load acting on the structure; $\boldsymbol{M}$, $\boldsymbol{C}$, and $\boldsymbol{K}$ are the concentrated mass matrix, damp matrix and stiffness matrix respectively.

Especialy $\boldsymbol{K} = \boldsymbol{K}_0 + \boldsymbol{K}_\sigma$. $\boldsymbol{K}_0$ is a line stiffness matrix whileas $\boldsymbol{K}_\sigma$ is an initial stress matrix or geometry stiffness matrix. $\boldsymbol{C} = \boldsymbol{M}\left(\sum_{i=1}^{N} 2\omega_i\xi_i\boldsymbol{\delta}_{0i}\boldsymbol{\delta}_{0i}^T\right)\boldsymbol{M}$. To reflect the real damp character of the structure, N should be large enough. Considering the computer capacity, N is chosen as 165 here. ω_i and ξ_i are the natural frequency and damp ratio, and $\boldsymbol{\delta}_{0i}$ is a nomal modal vector.

Since the structure contains long cables, many low natural frequencies exist. Table 1 lists the lowest five natural frequencies. Table 1 illustrates that the cable-clog systems will increse the structural stiffness.

4.3 Time history of the structure vibration

Frequency-domain analysis is suit for linear structures. To make a nonlinear analysis precisely, time-domain analysis has to be made (Wang 1994). Along-wind velocity is considered as an ergodic stationary random process and samples of the wind velocity related to time are generated by Eq. (22). Exerting wind forces on the structure with a mean velocity of 17 m/s which is the largest one in the site. For a sample of the wind velocity persisting 60 seconds, the nonlinear dynamic Eq. (42) is integrated directly by Newmark-β method using ADINA.

Among all the cabin nodes, the suspension point B_4 (in Fig. 2) has the largest vibration displacement. Fig. 10 shows the time history of displacement of the point B_4 and the left and right parts correspond to the six-cable and nine-cable structures respectively.

From Fig. 10, the cable-clog systems decrease the maximum displacement of the point B_4 from 70 centimeters to 7 centimeters. Because the wind velocity blows in the direction of axis X, the displacement along axis X is the largest one. Corresponding to axes X, Y, and Z, the ratio of displacement means of B_4 between the six-cable and the nine-cable structures is $|\bar{\mu}_6/\bar{\mu}_9| = (243.41, 6.87, 5.46)$.

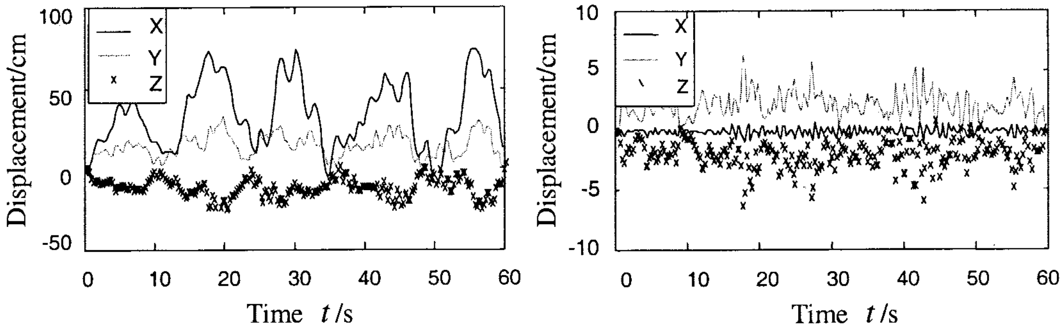

(a) Six-cable structure (b) Nine-cable structure

Fig. 10 Time history of displacement of the point B_4

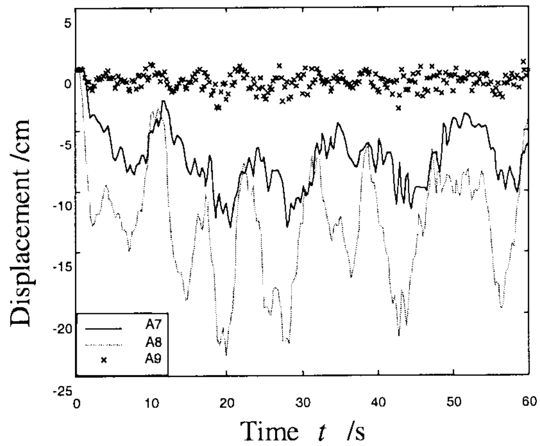

Fig. 11 Time histories of displacement of the lower ends A_7, A_8, and A_9

Fig. 11 shows the time history of displacement of the lower ends A_7, A_8, and A_9 of the passive cables. These displacements are in the directions of tangent at pulley A_7, A_8, and A_9 respectively. Since the lengths of the three passive cables are $l_7 = 318.03$ m, $l_8 = 234.18$ m, and $l_9 = 185.03$ m respectively when the cabin is balanced at the point D_2, the cable A_9B_9 is stretched most tightly and the displacement of the end A_9 is the smallest one. In addition, the orientation of the cable A_8B_8 is consistent with along-wind direction nearly, the vibration of the end A_8 contains the translation in the along-wind direction and vibration caused by turbulence.

4.4 Power spectral density of the responses

The response spectrum of displacement at point B_4 can be obtained using FFT transformation from the corresponding time history. The left and right parts in Fig. 12 describe the spectra corresponding to the six-cable and nine-cable structures respectively. It can be found that the cable-clog systems not only absorb the vibration energy at lower frequency band considerably but also

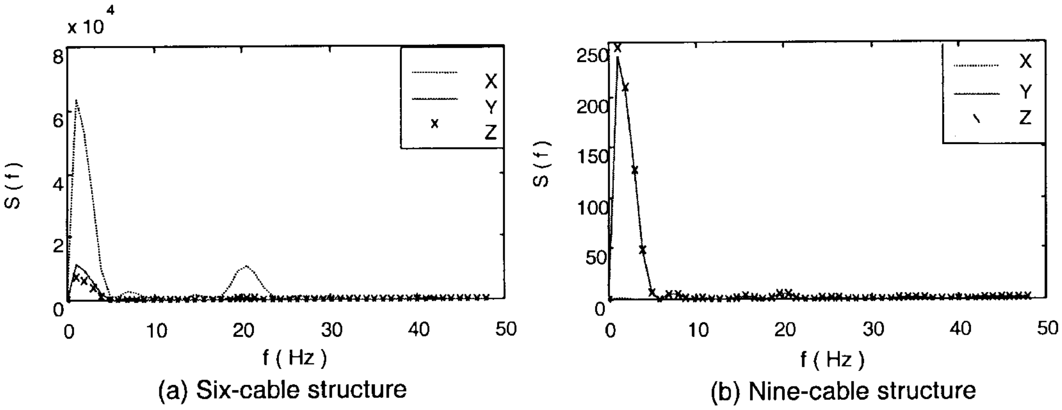

Fig. 12 Power spectrum density of displacement of the point B_4

constrain the vibration energy at higher frequency band.

5. Conclusions

From the above discussion, we may come to the following conclusions:

The cable tensions are sensitive to the orientation angle θ of the cabin. Optimization on cable tension distribution related to θ is necessary to benefit the computer control and ensure smooth movement.

It is necessary to utilize some measures to control the structural vibration of the cable-cabin structure. The three cable-clog systems absorb much vibration energy of the cable-cabin structure and transform the energy into the vibration of clogs massively. Therefore the wind-induced vibration of the cable-cabin structure is constrained significantly.

Although the cable-clog system constrains the structural vibration effectively, the maximum displacement of the feed may not satisfy the precision requirement, i.e., the maximum displacement of the feed being away from theoretical position may not be able to be less than 4 millimeters. For the sake of this, a parallel manipulator, Stewart platform, is amounted in the feed cabin as a feed position-fining platform (Su 2000). The initial fining made by the six active cables and the second fining made by Stewart platform compose a two-level adjusting system, and by this adjusting system the precision requirement on position and orientation of the feed may be assured.

References

Duan, B.Y. (1999), "A new design project of the line feed structure for large spherical radio telescope and its nonlinear dynamic analysis", *J. Mechatronics*, **9**(1), 53-64.

Duan, B.Y. (1999), "Integrated design with mechanical, electronic and optical technologies for the new generation large spherical radio telescope", *J. China Mech. Eng.* (in Chinese), **10**(9), 1002-1004.

Li, H. (1998), "China hopes to move FAST on largest telescope", *J. Science*, **281**(5378), 771.

Li, Q. and Cao, H. (1999), "Optimal design of wind-induced vibration control of tall buildings and high-rise structures", *J. Wind Struct.*, **2**(1), 69-83.

Su, Y.X. and Duan, B.Y. (2000), "Application of Stewart platform in the next generation large radio telescope", *J. Robotic Syst.*, **17**(7), 375-383.

Wang, Y.C. (1999), "Effect of cable stiffness on a cable-stayed bridge", *J. Struct. Eng. Mech.*, **8**(1), 27-38.

Wang, Z.H. (1994), "Simulation of wind loading", *J. Architectural Struct.* (in Chinese), **15**(1), 44-52.

Zhang, X.T. (1985), *Calculations on Structural Wind Press and Wind-induced Vibration* (in Chinese), Shanghai Tongji University Press.